Restricted Segmental Mobility Can Facilitate Medium-Range Chain Diffusion: A NMR Study of Morphological Influence on Chain Dynamics of Polyethylene

Y.-F. Yao,[†] R. Graf,[†] H. W. Spiess,*[,†] and S. Rastogi[†,‡]

Max-Planck-Institute for Polymer Research, Ackermannweg 10, 55128 Mainz, Germany, and Department of Chemical Engineering, Eindhoven University of Technology, P.O. Box 513, 5600MB Eindhoven, The Netherlands

Received December 18, 2007; Revised Manuscript Received February 7, 2008

ABSTRACT: The influence of the morphology on the local motion in the noncrystalline regions and chain diffusion between crystalline and noncrystalline regions is studied in ultrahigh molecular weight linear polyethylene: The behaviors of samples of the same material crystallized from the melt and from solution are compared. The geometrical restrictions of the conformational transitions are probed via anisotropic NMR interactions, i.e., $^{13}C-^{1}H$ dipole–dipole couplings and ^{13}C chemical shift anisotropy. As they are averaged out under MAS, recoupling techniques are applied to yield sideband patterns or quasi-static NMR spectra, from which residual anisotropies are determined. Chain diffusion is probed by ^{13}C exchange NMR. As expected, the local conformational transitions are more restricted in the solution crystallized sample compared with the melt crystallized one. Moreover, the motional narrowing observed by both techniques indicates that the local mobility in the noncrystalline regions of the solution crystallized sample consists mainly of effectively axial motion of extended trans-conformers around their local chain axes. This facilitates the chain diffusion between the crystalline and the noncrystalline regions, being significantly faster in solution crystallized compared to melt crystallized samples, where the local mobility is much more isotropic. The implications of these results for the understanding of crystal thickening and cold drawing are discussed.

Introduction

The material properties of solid polymeric materials are often governed by molecular dynamics on different time and length scales.[1] Detailed knowledge of molecular dynamics is important for understanding the origin of such properties. Molecular dynamics in polymers is influenced not only by the chemical structure of the macromolecule but also by the spatial arrangement of the polymer chains in a given morphology. Different packing arrangements give rise to different spatial restrictions, which in turn manifest themselves in the dynamic behavior of the polymer chains.[2−5] Because of the connectivity of the building units, local and long-range dynamics are coupled[6,7] and the sample morphology can influence both of them. However, the morphological influence on chain dynamics is usually not so easy to observe because it is difficult to distinguish from that of the chemical structure. In this context polyethylene (PE) is a good candidate for the study of morphological influence due to its simple chemical structure.

The morphology of semicrystalline polymers varies with the crystallization conditions,[8,9] where melt and solution crystallization are common ways to change the sample morphology. Linear PE crystallized from very dilute solution forms a layered chain-folded morphology; i.e., the polymer chains fold back and forth to form crystals, and the chain folds represent the noncrystalline regions.[10,11] When the same sample is crystallized from the melt, a switchboard-like morphology, where the individual chains go from one to the next crystalline layer, is more likely.[12,13] Sample morphologies developed from different crystallization conditions have been used to explain the different behavior in the crystal thickening[14,15] and mechanical deformation.[15,16] Comparing the morphologies of melt and solution crystallized PE samples, one may conclude that their major difference usually lies in the noncrystalline regions, i.e., the amount of noncrystalline material, the chain arrangement, and the resultant chain dynamics. The noncrystalline phase in PE also plays an important role in the melting and related chain dynamics.[17,18] Most of this knowledge comes from thermal analysis and X-ray scattering as well as mechanical relaxation measurements.[1]

Spectroscopic methods are also able to elucidate the chain organization and dynamics. In particular, solid-state NMR is a very suitable technique for the study of chain dynamics in semicrystalline polymers.[4,19,20] This is due to its ability to monitor the chain dynamics simultaneously on different length and time scales. Local chain dynamics of PE in crystalline[21,22] and noncrystalline regions, as well as the chain diffusion between them,[23,24] have been studied extensively. It has been found that the local chain dynamics in the crystalline regions is a well-defined 180° jump motion. The local chain dynamics in the noncrystalline regions is conformationally restricted at ambient temperatures and approaches an almost random chain motion only close to the melting point. Moreover, at ambient temperatures the chains diffuse between crystalline and noncrystalline regions on a time scales of minutes. Thus, chain diffusion can be considered as medium-range chain dynamics.

In this paper, we will correlate the different kinds of chain dynamics in PE directly. It will be demonstrated that the morphology strongly influences both the local chain dynamics in the noncrystalline regions and the chain diffusion between noncrystalline and crystalline regions in an intriguing way.[24] The purpose of this work, therefore, is to elucidate the morphological influence on the chain dynamics in detail in order to provide a better basis for the understanding of various material properties on a microscopic level. Some of the polymer physics aspects of this study have recently been published in a Rapid Communication[25] and are briefly reviewed for the reader's convenience.

* To whom correspondence should be addressed.
[†] Max-Planck-Institute for Polymer Research.
[‡] Eindhoven University of Technology.

10.1021/ma702815k CCC: $40.75
Published on Web 03/13/2008

Experimental Section

The linear polyethylene studied in this work has an average molar mass of 4600 kg/mol. Solution crystallized samples were prepared from dilute solutions in xylene having 1 wt % of polyethylene.[26] The high molar mass of polyethylene forms a viscous solution, which on cooling becomes a gel. The gel was stapled on a cardboard to avoid any shrinkage during solvent evaporation, which took nearly a week. Melt crystallized samples were prepared on cooling the melt of the solution crystallized samples at a rate of 10 K/min. The linearity of sample is quantified by determining the branching degree to be less than 1 CH_2 per 100 000 CH_2 by ^{13}C melt-state NMR measurements.[27] The solution crystallized sample has a crystallinity of 76% as opposed to 44% for the melt crystallized sample. The thickness of the crystallites for the solution crystallized sample is 11.9 nm determined by longitudinal acoustic mode (LAM) Raman spectroscopy.[14] In the melt crystallized samples, the crystal thickness varies slightly depending on the crystallization procedure.

All solid-state NMR studies reported in this paper have been performed at a Bruker DSX spectrometer operating at 500.13 MHz ^1H Larmor frequency. Advanced NMR recoupling techniques correlating isotropic chemical shifts observed under magic angle spinning (MAS) condition with motional averaged anisotropic interactions, i.e., $^1H-^{13}C$ heteronuclear dipole–dipole coupling and ^{13}C chemical shift anisotropy (CSA), have been used to study the local chain dynamics in the samples. The measurement of $^1H-^{13}C$ heteronuclear dipole–dipole couplings was achieved by the rotor encoded REDOR (ReREDOR) experiment.[28] For the ReREDOR experiments a commercial 2.5 mm MAS double-resonance probe was used at a spinning frequency of 25 kHz. The recoupling of ^{13}C CSA was achieved by the SUPER technique.[29] In this case a 4 mm MAS double-resonance probe was used at a spinning frequency of 3 kHz. The same probe was used to study the chain diffusion between noncrystalline and crystalline regions based on a ^{13}C exchange type experiment[23] under magic angle spinning at 6 kHz. The 90° pulse length in the 2.5 mm MAS probe was adjusted to 2.5 μs on both channels, corresponding to a RF spin nutation frequency $\omega_1/2\pi = 100$ kHz. The 90° pulse length in the 4 mm MAS probe varies between 3 and 4 μs on both channels, corresponding to $\omega_1/2\pi = 63$–83 kHz. In all ^{13}C-detected experiments, CW or TPPM[30] decoupling was applied for heteronuclear dipolar decoupling. The decoupling power level was 83–89 kHz for the 4 mm MAS probe and 100 kHz for the 2.5 mm MAS probe. A variable amplitude CP, with the RF power being ramped from 80 to 100% on the proton channel, was used for the experiments involving a cross-polarization step. The temperature of the bearing gas was varied for temperature-dependent experiments. Temperature and absence of temperature gradients were checked with $Pb(NO_3)_2$ under the same spinning conditions. In all cases, particular care has been taken using appropriate experimental repetition delays and phase cycling to avoid signal contributions from transient NOE effects.[31,32]

Results

Segmental Mobility in the Noncrystalline Regions. The segmental mobility can be probed by ^{13}C NMR in various ways. All are based on the fact that conformational motions with correlation times below 10 μs average the local interactions determining the NMR spectrum: (i) The presence of different local conformers and exchange between them is reflected in the isotropic chemical shift accessible in ^{13}C MAS NMR spectra. (ii) Geometrical restrictions of the conformational transitions are probed via anisotropic NMR interactions, i.e., $^{13}C-^1H$ dipole–dipole couplings, which yield similar information as ^2H NMR and ^{13}C chemical shift anisotropy, CSA. Since they are averaged out under MAS, recoupling techniques must be applied to yield sideband patterns or quasi-static NMR spectra, from which residual anisotropies can be determined.

Figure 1a,b shows ^{13}C-CP/MAS spectra of the solution and the melt crystallized samples at $T = 320$ K, which is above the static glass transition temperature of PE.[33] In the spectra, the signals observed at ~33 ppm with identical line width are assigned to all-trans conformations in crystalline regions of samples.[34] In contrast, chain segments in the noncrystalline regions of PE are able to adopt various conformations, and the molecular dynamics present in these areas leads to a fast exchange between these conformations. The NMR signal thus shows a peak at about 31 ppm; the position and width depend on the conformational statistics and the accessibility of the conformational space to dynamic processes present in the noncrystalline areas.[32] Comparing the spectra of the samples, clear differences are observed in the noncrystalline signals. The spectrum of the solution crystallized sample shows a broad noncrystalline peak (Δfwhh = 2.46 ppm) at 31.1 ppm, whereas the noncrystalline signal of the melt crystallized sample exhibits a sharper peak (Δfwhh = 0.99 ppm) at 30.9 ppm. This may reflect differences in the conformations and/or molecular dynamics of the chain segments in these regions, whose behavior clearly shows a marked dependence on the crystallization procedure and the resultant morphology.

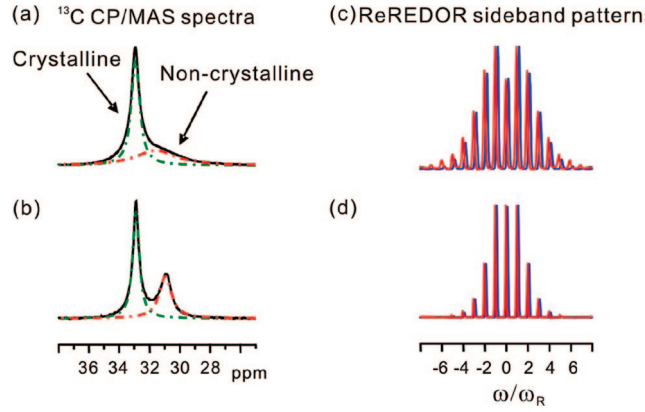

Figure 1. ^{13}C CP/MAS spectra (6 kHz MAS, 2 ms CP contact) of PEs and ReREDOR sideband patterns (25 kHz MAS, 3 rotor periods recoupling) from the noncrystalline regions, recorded at $T = 320$ K. The ^{13}C CP/MAS spectra of (a) solution crystallized and (b) melt crystallized PE show two components, the noncrystalline signal (~31 ppm, red dashed line) and the crystal peak (~33 ppm, green dashed line). The ReREDOR sideband pattern of noncrystalline (c, red line) solution crystallized and of noncrystalline (d, red line) melt crystallized PE. The underlying blue patterns are simulations with a dipole–dipole coupling constant of $D_{IS}/2\pi = 9.1$ kHz for the solution crystallized sample and 6.3 kHz for the melt crystallized sample.

A quantitative way to study the local chain dynamics in the noncrystalline regions of PE is to monitor the heteronuclear dipole–dipole coupling. The heteronuclear dipole–dipole coupling may differ due to different segmental mobility caused by dynamic processes of the polymer chains in the noncrystalline areas. To quantify the heteronuclear dipole–dipole coupling, the rotor encoded REDOR recoupling sequence has been applied.[28] The resulting ReREDOR sideband patterns for the two samples taken at the isotropic chemical shift of the noncrystalline signals are shown in Figure 1c,d. The broad profile of the ReREDOR sideband pattern of the noncrystalline regions in the solution crystallized sample compared to the melt crystallized sample is indicative of stronger dipole–dipole coupling in the solution crystallized sample.[25,35] The quantitative analysis of the recoupled sideband patterns yields an effective residual heteronuclear coupling constant of 9.1 kHz for the noncrystalline components in the solution crystallized sample compared to 6.3 kHz for the melt crystallized sample. These values correspond to dynamic local order parameters of 0.43 and 0.30,[36] respectively. The higher dynamic local order parameter in the solution crystallized sample results from a more anisotropic molecular

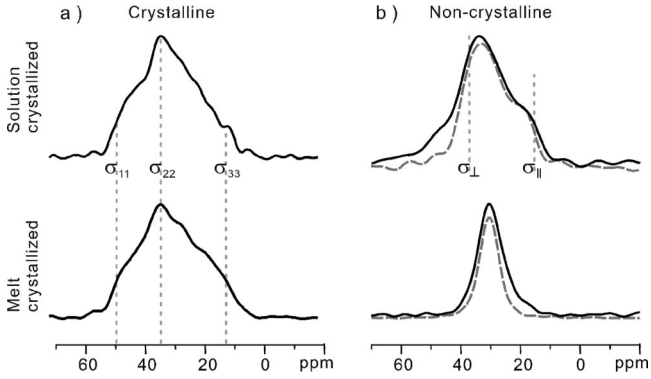

Figure 2. ^{13}C chemical shift anisotropy (CSA) static powder line shape of the two PEs: (a) the crystalline pattern and (b) the noncrystalline pattern. These patterns are taken from the slices of SUPER experiments,[28] measured at 3 kHz MAS and $T = 320$ K. Spectra given in solid black lines were measured with $^{1}H-^{13}C$ cross-polarization; those given in dashed gray lines were measured via ^{13}C single pulse excitation.

motion and thus is indicative of a more restricted local chain dynamics in the noncrystalline regions of the sample.

More detailed geometrical information on the dynamic processes can be obtained from the static powder line shape of the ^{13}C chemical shift anisotropy (CSA). Therefore, a CSA recoupling scheme has been applied to obtain the static CSA pattern for the noncrystalline regions separated from the static line shape of crystalline PE. The CSA patterns of the two samples recorded at $T = 320$ K are shown in Figure 2. The patterns of the crystalline components (Figure 2a) are very similar for the two samples, whereas significant differences are observed for the noncrystalline components (Figure 2b). The CSA powder line shape of the noncrystalline region in the solution crystallized sample shows features of an axially symmetric CSA tensor, whereas the CSA pattern of the noncrystalline region of the melt crystallized sample is lacking the typical features of a tensorial powder line shape. It rather resembles a broadened isotropic line. These results indicate that the chains in the noncrystalline regions of the solution crystallized sample undergo a more restricted anisotropic motion close to a locally axial rotation around the chain backbone, whereas the chains in the melt crystallized sample show a more isotropic motion. Note that the CSA in the noncrystalline regions of the solution crystallized sample has a $\sigma_{||} \approx \sigma_{33}$, whereas $\sigma_{\perp} \approx (\sigma_{11} + \sigma_{22})/2$ (see below). The CSA line shape recorded for different slices within the broad resonance did not show significant variation.

In the literature, the presence of an interphase of intermediate order between the noncrystalline and the crystalline phases has been proposed on the basis of both theoretical and experimental considerations. In solid-state NMR, this aspect can be addressed varying the initial source of polarization for the CSA recoupling experiment. If the experiment is started with an initial cross-polarization (CP) step using a short contact time, the acquired signal results predominantly from sites with a stronger heteronuclear dipole–dipole coupling. In the case of PE, such rather immobile sites are in close proximity to crystalline areas. In contrast, the signals in single pulse experiments with short relaxation delay (2 s) result from more mobile areas of the sample due to the long ^{13}C T_1 relaxation time of crystalline polyethylene ($T_1 > 1000$ s).[37] The powder line shapes of the noncrystalline areas of the solution crystallized sample acquired with both experimental approaches match very well, indicating that the observed restricted anisotropic dynamics of the noncrystalline areas in the solution crystallized sample is characteristic of these regions as a whole. In the case of the melt crystallized sample, the Lorenzian line shape obtained from the CP method is somewhat broader than that obtained from single pulse excitation; however, the line shape stays Lorenzian and does not show any features of a powder line shape resulting from an axial-symmetric averaged CSA tensor as observed in the case of the solution crystallized sample. Combining the results from heteronuclear dipole–dipole and CSA recoupling experiments, we conclude that at ambient temperature the conformational exchange in the noncrystalline areas of the solution crystallized sample is highly restricted whereas the polymer chain in the melt crystallized sample can explore a much larger fraction of the conformational space, leading to a more isotropic segmental dynamics.

Chain Diffusion between Noncrystalline and Crystalline Regions in PE. To investigate the influence of the local chain mobility on the cooperative chain motion between the crystalline and the noncrystalline regions, i.e., the chain diffusion, 1D ^{13}C exchange spectra have been recorded for both samples.

The very long ^{13}C T_1 relaxation times in the crystalline regions[37] and the much shorter ^{13}C T_1 relaxation time in the noncrystalline regions of PE (~0.6 s) facilitate the observation of chain translation motion between the crystalline and the noncrystalline regions by exchange NMR.[23] If the time window chosen in the experiment is significantly shorter than the T_1 relaxation times in the crystalline regions of PE, the increase of polarization in crystalline regions cannot originate from simple T_1 relaxation of the crystalline chain units but has to be attributed to the chain translational motion, which transfers polarized noncrystalline chain units into crystalline regions of the sample. These chain units then adopt the all-trans conformation and thus the chemical shift of the crystalline area and finally contribute to the crystalline signal in the spectrum.[23] The experimental scheme for the ^{13}C exchange NMR method used in this work is similar to the saturation recovery method, often used in NMR to determine T_1 relaxation times. As long as the exchange or relaxation delay is significantly shorter that the T_1 relaxation time of crystalline polyethylene, the chain diffusion between crystalline and noncrystalline regions can be monitored via observing the increase of polarization in the crystalline regions. Figure 3a shows a series of NMR spectra varying with different exchange time. These spectra were recorded with the 1D ^{13}C exchange experiment at $T = 320$ K, where the mechanical α-relaxation indicates hopping rates of the crystalline stems around 20 Hz.[1,23]

In the melt crystallized sample the initial buildup of the signal arises with the relaxation process of the noncrystalline region in the magnetic field of the spectrometer. In the solution crystallized sample, however, with increasing waiting time two peaks are observed. The peak positions match with those of the noncrystalline and the crystalline regions. The intensity of the crystalline peak increases rapidly with the exchange time. Considering the long relaxation times of the crystalline component, the buildup of the crystalline signal has to be attributed to the translation motion of the chain segments from the noncrystalline to the crystalline regions. The same phenomenon, though very weak, is also observed in the melt crystallized samples at the largest exchange time of 40 s.

When combined with the data reported above, it can be conclusively stated that though local chain dynamics in the noncrystalline region of the solution crystallized sample is restricted, the motional anisotropy present in the noncrystalline region favors the chain diffusion between crystalline and noncrystalline regions.[25] On the contrary, for the melt crystallized sample though local chain dynamics is high, hardly any chain diffusion between the crystal and the noncrystalline region is observed under the same conditions. These observations at ambient temperatures appear counterintuitive at first sight.

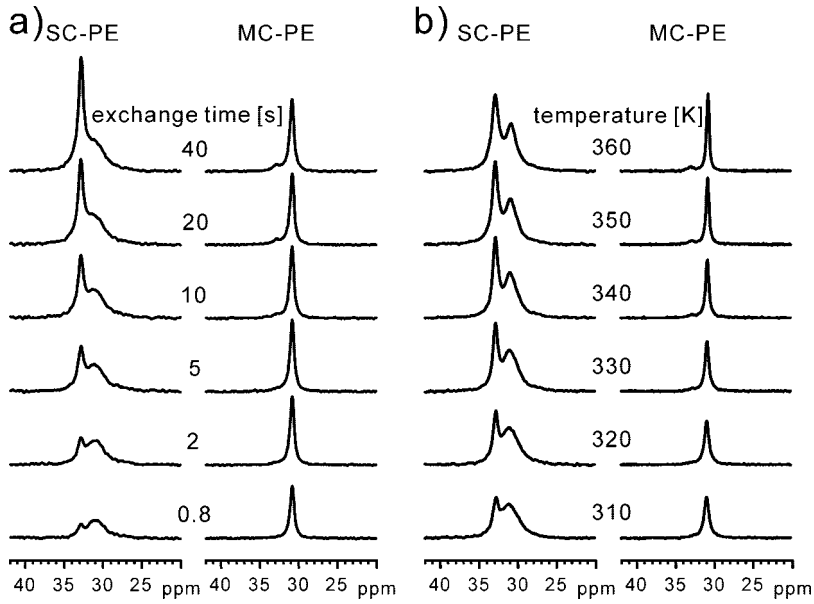

Figure 3. ^{13}C MAS exchange spectra of the solution crystallized sample (SC-PE) and the melt crystallized sample (MC-PE): (a) measured at 6 kHz MAS, $T = 320$ K with different exchange times; (b) measured at 6 kHz MAS, a fixed exchange time (5 s), and with different experimental temperatures.

The exchange process in linear melt crystallized polyethylenes has been reported earlier by Schmidt-Rohr and Spiess.[23] Figure 3b shows the exchange process at different temperatures at fixed exchange time of 5 s. With increasing temperature, the exchange process starts appearing in the melt crystallized sample, but it is much more pronounced in the solution crystallized sample at all temperatures. As shown in our own recent Communication,[25] the chain diffusion coefficient for the solution crystallized sample is 20 times larger than that of the melt crystallized one in the entire temperature range studied. This was attributed to an entropic difference of the transition state. Therefore, we now consider the temperature dependence of the local chain dynamics in the noncrystalline regions of the two samples.

Temperature Dependence of the Local Chain Dynamics in the Noncrystalline Regions. Figure 4 shows the ReREDOR sideband patterns for the noncrystalline regions of the samples at different temperatures. The corresponding $^{1}H-^{13}C$ dipole–dipole couplings are listed in Table 1. The most remarkable observation from these ReREDOR experiments is that for the solution crystallized sample the residual $^{1}H-^{13}C$ dipole–dipole coupling hardly changes with increasing temperature, indicating that the motional anisotropy in the noncrystalline regions of the solution crystallized sample is maintained even at relatively high temperatures although the molecular dynamics is accelerated. In contrast, in the melt crystallized sample the residual $^{1}H-^{13}C$ dipole–dipole coupling decreases with increasing temperature, as expected for the increased molecular mobility at elevated temperatures and found previously in ^{2}H NMR studies of such samples.[19]

A similar phenomenon is observed in the ^{13}C CSA patterns of the noncrystalline regions at different temperatures, which are shown in Figure 5. The line shape of the ^{13}C CSA pattern of the solution crystallized sample always shows features of an axially symmetric CSA tensor at all temperatures, whereas the width of the resonance line in the melt crystallized sample decreases with increasing temperature, but the line shape always keeps the isotropic feature. This phenomenon further confirms that the motional anisotropy in the noncrystalline regions of the solution crystallized sample is maintained at relatively high temperatures.

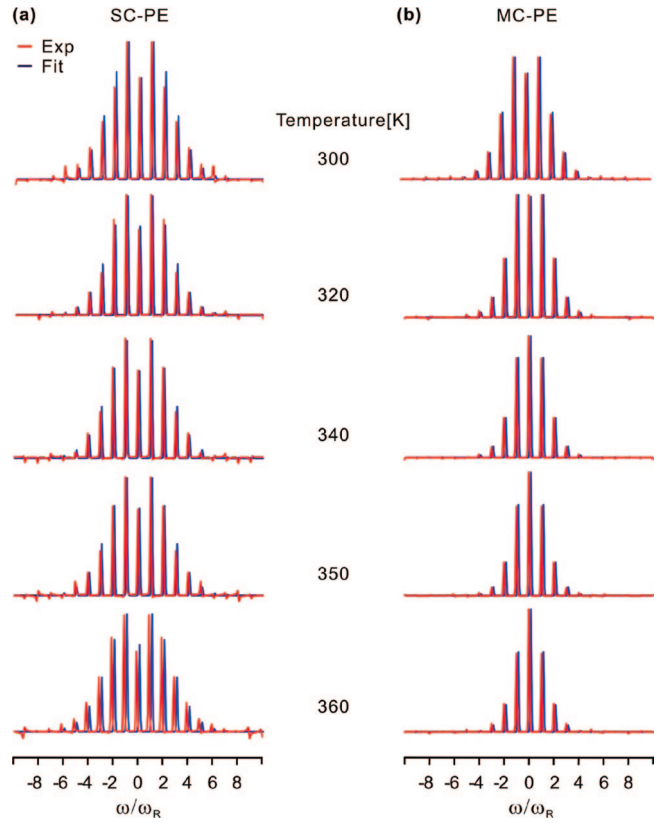

Figure 4. Temperature-dependent ReREDOR sideband patterns due to $^{1}H-^{13}C$ couplings in noncrystalline regions of the samples. SC-PE and MC-PE refer to the solution and the melt crystallized samples, respectively.

Discussion

Morphological Effects on the Local Chain Dynamics. The local chain dynamics is probed here via the ^{13}C CSA and the $^{1}H-^{13}C$ dipole–dipole coupling. For extended trans-conformations the z-principal axes of these anisotropic interactions are perpendicular to each other, as shown in Figure 6.[38,39] Motional narrowing of these interactions then provides particularly detailed information about the geometry of the local dynamics.[40]

Table 1. $^1H-^{13}C$ Dipole–Dipole Coupling Constant $D_{IS}/2\pi$ (kHz) in the Noncrystalline Regions of PEs at Different Temperatures[a]

temperature [K]	$D_{IS}/2\pi$ [kHz] of SC-PE	$D_{IS}/2\pi$ [kHz] of MC-PE
300	9.1	6.9
320	9.1	6.3
340	8.9	5.6
350	8.9	5.3
360	8.8	5.0

[a] These constants are from the simulations of the experimental spin sideband patterns.

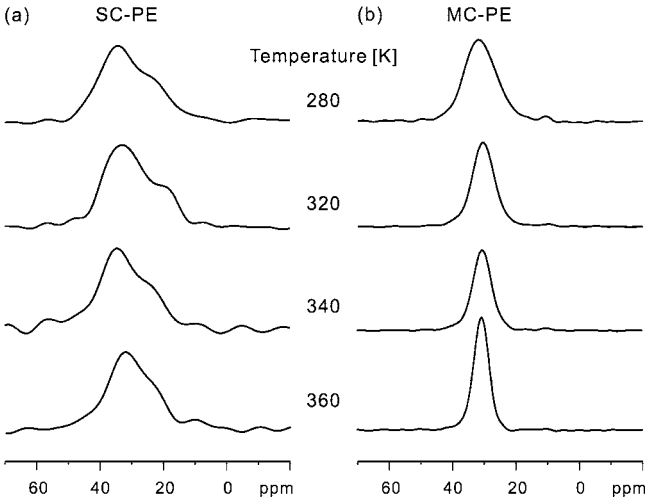

Figure 5. ^{13}C CSA static powder line shapes of signals from noncrystalline regions acquired at different temperatures, recorded as described for Figure 2.

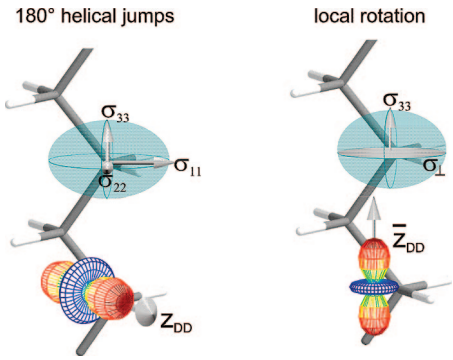

Figure 6. 180° jump motion vs rotation around the local chain axis probed by ^{13}C CSA and $^{13}C-^1H$ dipole–dipole coupling.

Rotations by 180° of the all-trans stems in the crystalline regions do not change the CSA tensor or the $^1H-^{13}C$ dipole–dipole coupling. Effectively axial motion of extended all-trans segments around their local chain axis, however, leads to an average axially symmetric CSA tensor, where σ_{33} does not change while σ_{11} and σ_{22} are averaged.[41] Precisely this kind of motional averaging is indeed observed for the noncrystalline regions of the solution crystallized sample (see Figures 2 and 5). It should be noted, however, that the anisotropy $\delta = \sigma_{||} - \sigma_{\perp}$ of the recorded axially symmetric CSA tensor is reduced by ~20% compared to the value obtained for a simple rotational motion around the z-axis of the CSA tensor.

The same type of axial motion results in an axially symmetric $^1H-^{13}C$ dipole–dipole coupling tensor with the unique axis along the local chain axis and reduced in strength by a factor of 2,[20,40] corresponding to a local dynamic order parameter of $S = 0.5$. The experimental value determined from the ReREDOR sideband pattern for the noncrystalline regions in the solution crystallized sample (see Figure 4a) at $T = 320$ K is $S = 0.43$,

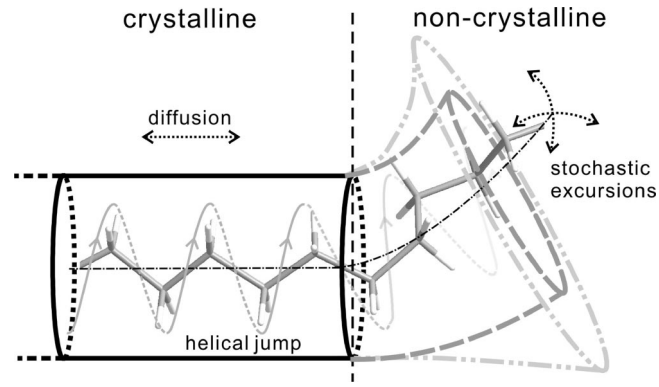

Figure 7. Illustration of chain motions in PE. The individual helical jump generates the translation of chain stem by one CH_2 unit. These initial translation steps evolve in the course of time into a diffusive motion between crystalline and noncrystalline regions, which is observed in the NMR experiments. The tubes represent spatial and dynamic restrictions of the PE chain due to its local environment.

i.e., lower by 14% than expected for a simple rotational motion around the local chain axis. Thus, both the motionally averaged CSA and dipole–dipole coupling indicate additional mobility with angular excursions around ±20°.[20,41] Thus, rotation of locally extended trans conformers seems to be the main possible chain motion of the chains in the noncrystalline regions of the solution crystallized sample. This model is further supported by the finding that additional reductions of the averaged tensorial coupling values, attributed to minor fluctuations of the local rotation axis, are consistent for both CSA and dipole–dipole coupling tensor. It should be noted, however, that the effectively axial motion deduced from the CSA line shapes and the dipole–dipole sideband patterns does not require complete rotation about the local chain axis. Large-amplitude rocking motions and occasional 180° flips will lead to similar spectra.[41,42]

Note, however, that the ^{13}C-MAS NMR spectrum of the solution crystallized sample exhibits a broad inhomogeneous line shape, indicating a significant distribution of folds rather than well-defined conformations as found in the cyclic alkanes.[43]

For the melt crystallized sample, the lower dynamic local order parameter (0.30 at 320 K) and even lower values at higher temperatures (see Figure 4b) indicate that the local fluctuations have larger amplitudes and involve more conformations leading to a more isotropic chain dynamics (see also ref 19). This consists well with the observation in the CSA pattern, where the static CSA powder line shape indicates an almost isotropic motion. For the investigated average molar mass above 1 million g/mol the predominant structure present in the noncrystalline regions of the melt crystallized sample, therefore, will be more random as described by the switchboard-like morphology, with comparatively low restrictions on the local chain dynamics.

Morphological Effects on the Chain Diffusion. For the medium range chain diffusion, our experimental results show that the solution crystallized sample exhibits much faster chain diffusion than the melt crystallized one.[25] This observation is rationalized in a cartoon picture of the chain dynamics shown in Figure 7. In this picture, a chain stem is moving between the noncrystalline region (right side) and the crystalline region (left side). The tube represents spatial and dynamic restrictions of the PE chain due to its environment, and the diameter of tube indicates the degree of restriction. In this model the chain diffusion is achieved by sliding of the chain stem in the tube. Because of the chain connectivity, the motion of the noncrystalline chain portion is connected to that of the chain portion in the crystallite. Taking into account that the chain diffusion in the crystal is always along the chain backbone, it is easy to imagine that motions in the noncrystalline regions involving

extended trans segments as indicated by CSA and $^{1}H-^{13}C$ dipole–dipole coupling in the solution crystallized sample are very effective for the chain diffusion, whereas random motions such as almost isotropic fluctuations of chain segments are not compatible with and may even be an obstacle for chain diffusion. Following this idea, reducing the motional degree of freedom of the noncrystalline chain motion, i.e., from random motion to the motion along the extended chain conformations, can favor chain diffusion. In thermodynamics terms, the reduction of the motional degrees of freedom of the chain motion in fact is lowering the entropy change involved in the translational motion from the crystalline to the noncrystalline environment. Hence, besides the activation enthalpy which relates to the change of chain conformation involved in the motion, apparently the entropy change in the chain diffusive motion also plays an important role.[25] This gives a plausible explanation why in the solution crystallized sample locally restricted chain mobility can be in accord with efficient chain diffusion on a much longer time scale. Further experimental confirmation of these conjectures as well as a study of the influence of chain branches is the subject of ongoing studies in our laboratory.

One can also imagine that the differences of the chain diffusivity might be due to differences in the motions occurring in the crystallites. In the literature, defect-driven mechanisms have been proposed to explain the translation of an extended all-trans chain through a PE crystallite.[44] In this scenario, a defect is created, e.g., at one side of the crystal, and the translational motion is accomplished, when the defect has moved to the other side and left the crystallite. If, however, the defect only travels inside the crystallite, is reflected back, or annihilated, it will not lead to translational motion of the stem but will still cause local reorientation of the CH_2 units. Thus, local jump rates may differ from the effective jump rate responsible for chain diffusion. As shown in ref 25, this is indeed the case, especially at elevated temperatures, where the jump rates are in the range of tens of kilohertz. It would be elucidating to compare the local and the effective jump rates in the same solution crystallized and melt crystallized samples. Unfortunately, however, such data are not available, as doubly ^{13}C-labeled samples are required.[21,22]

Conclusions

The above observations when combined together clearly demonstrate that the restricted local chain mobility present in the noncrystalline region of solution crystallized PE plays a crucial role for the chain diffusion between noncrystalline and crystalline regions. The absence of such restrictions in the melt crystallized sample of the chemically identical polymer shows suppressed cooperative motion from noncrystalline to crystalline regions. This has important implications for our understanding of crystal thickening. For example, the solution crystallized sample shows enhanced chain mobility along the crystallographic *c*-axis, which when combined with the regular stacking of crystals ultimately leads to the doubling of the initial crystal thickness.[14] In contrast, crystals in melt crystallized samples of the same material hardly thicken. Moreover, the motional anisotropy present in the noncrystalline regions of the solution crystallized sample is suggestive of the observed easy mechanical deformation of the crystals in the solid state,[16] which is indicative for the adjacent re-entry structure. Melting kinetics observed in the solution crystallized samples also support these observations.[18]

Finally, we would like to state that the observations reported in this paper on a specific polymer, ultrahigh molecular weight PE, may have much more general implications. The reported differences in the dynamic behavior of noncrystalline regions in semicrystalline polymers and the resulting entropic contribution controlling the chain translation motion in crystalline areas might be crucial for the mechanical performance and the long-term stability of semicrystalline polymers in general.

References and Notes

(1) Ward, I. M.; Hadley, D. W. *An Introduction to the Mechanical Properties of Solid Polymers*, 2nd ed.; John Wiley and Sons: London, 1993.
(2) Uehara, H.; Yamanobe, T.; Komoto, T. *Macromolecules* **2000**, *33*, 4861–4870.
(3) Axelson, D. E.; Russell, K. E. *Prog. Polym. Sci.* **1985**, *11*, 221–282.
(4) Packer, K. J.; Pope, J. M.; Yeung, R. R.; Cudby, M. E. A. *J. Polym. Sci., Polym. Phys. Ed.* **1984**, *22*, 589–616.
(5) Chen, Q.; Yamada, T.; Kurosu, H.; Ando, I.; Shiono, T.; Doi, Y. *J. Polym. Sci., Polym. Phys. Ed.* **1992**, *30*, 591–601.
(6) Doi, M.; Edwards, S. F. *The Theory of Polymer Dynamics*; Oxford University Press: Oxford, 1986.
(7) Kimmich, R.; Fatkullin, N. *Adv. Polym. Sci.* **2004**, *170*, 1–113.
(8) Gedde, U. W.; Mattozzi, A. *Adv. Polym. Sci.* **2004**, *169*, 29–74.
(9) Ungar, G.; Zeng, X. B. *Chem. Rev.* **2001**, *101*, 4157–4188.
(10) Organ, S. J.; Keller, A. *J. Mater. Sci.* **1985**, *20*, 1571–1585.
(11) Weber, C. H. M.; Chiche, A.; Krausch, G.; Rosenfeldt, S.; Ballauff, M.; Gottker-Schnetmann, I.; Tong, Q.; Mecking, S.; Harnau, L. *Nano Lett.* **2007**, *7*, 2024–2029.
(12) Flory, P. J. *J. Am. Chem. Soc.* **1962**, *84*, 2857–2867.
(13) Flory, P. J.; Yoon, D. Y.; Dill, K. A. *Macromolecules* **1984**, *17*, 862–868.
(14) Rastogi, S.; Spoelstra, A. B.; Goossens, J. G. P.; Lemstra, P. J. *Macromolecules* **1997**, *30*, 7880–7889.
(15) Rastogi, S.; Terry, A. E. *Adv. Polym. Sci.* **2005**, *180*, 161–194.
(16) Smith, P.; Lemstra, P. J.; Pijpers, J. P. L.; Kiel, A. M. *Colloid Polym. Sci.* **1981**, *259*, 1070–1080.
(17) Rastogi, S.; Lippits, D. R.; Hohne, G. W. H.; Mezari, B.; Magusin, P. *J. Phys.: Condens. Matter* **2007**, *19*, 205122.
(18) Lippits, D. R.; Rastogi, S.; Hohne, G. W. H. *Phys. Rev. Lett.* **2006**, *96*, 218303.
(19) Hentschel, D.; Sillescu, H.; Spiess, H. W. *Macromolecules* **1981**, *14*, 1605–1607.
(20) Schmidt-Rohr, K.; Spiess, H. W. *Multidimensional Solid-State NMR and Polymers*; Academic Press: London, 1994.
(21) Hu, W. G.; Boeffel, C.; Schmidt-Rohr, K. *Macromolecules* **1999**, *32*, 1611–1619.
(22) Schnell, I.; Watts, A.; Spiess, H. W. *J. Magn. Reson.* **2001**, *149*, 90–102.
(23) Schmidt-Rohr, K.; Spiess, H. W. *Macromolecules* **1991**, *24*, 5288–5293.
(24) Klein, P. G.; Robertson, M. B.; Driver, M. A. N.; Ward, I. M.; Packer, K. J. *Polym. Int.* **1998**, *47*, 76–83.
(25) Yao, Y.-F.; Graf, R.; Spiess, H. W.; Rastogi, S.; Lippits, D. R. *Phys. Rev. E* **2007**, *76*, 060801(R) .
(26) Rastogi, S.; Spoelstra, A. B.; Goossens, J. G. P.; Lemstra, P. J. *Macromolecules* **1997**, *30*, 7880–7889.
(27) Klimke, K.; Parkinson, M.; Piel, C.; Kaminsky, W.; Spiess, H. W.; Wilhelm, M. *Macromol. Chem. Phys.* **2006**, *207*, 382–395.
(28) Saalwaechter, K.; Schnell, I. *Solid State Nucl. Magn. Reson.* **2002**, *22*, 154–187.
(29) Liu, S. F.; Mao, J. D.; Schmidt-Rohr, K. *J. Magn. Reson.* **2002**, *155*, 15–28.
(30) Bennett, A. E.; Rienstra, C. M.; Auger, M.; Lakshmi, K. V.; Griffin, R. G. *J. Chem. Phys.* **1995**, *103*, 6951–6958.
(31) Lyerla, J. R.; VanderHart, D. L. *J. Am. Chem. Soc.* **1976**, *98*, 1697–1700.
(32) Earl, W. L.; Vanderhart, D. L. *Macromolecules* **1979**, *12*, 762–767.
(33) Davis, G. T.; Eby, R. K. *J. Appl. Phys.* **1973**, *44*, 4274–4281.
(34) Vanderhart, D. L. *J. Magn. Reson.* **1981**, *44*, 117–125.
(35) Cho, T. Y.; Shin, E. J.; Jeong, W.; Heck, B.; Graf, R.; Strobl, G.; Spiess, H. W.; Yoon, D. Y. *Macromol. Rapid Commun.* **2006**, *27*, 322–327.
(36) Demus, D.; Goodby, J. W.; Gray, G. W.; Spiess, H. W.; Vill, V. *Handbook of Liquid Crystals*; Wiley-VCH: Weinheim, 1998.
(37) Axelson, D. E.; Mandelkern, L.; Popli, R.; Mathieu, P. *J. Polym. Sci., Part B: Polym. Phys.* **1983**, *21*, 2319–2335.
(38) VanderHart, D. L. *J. Chem. Phys.* **1976**, *64*, 830–834.
(39) Opella, S. J.; Waugh, J. S. *J. Chem. Phys.* **1977**, *66*, 4919–4924.
(40) Graf, R.; Ewen, B.; Spiess, H. W. *J. Chem. Phys.* **2007**, *126*, 041104.
(41) Macho, V.; Brombacher, L.; Spiess, H. W. *Appl. Magn. Reson.* **2001**, *20*, 405–432.
(42) Wind, M.; Graf, R.; Heuer, A.; Spiess, H. W. *Phys. Rev. Lett.* **2003**, *91*, 155702.
(43) Moeller, M. *Adv. Polym. Sci.* **1985**, *66*, 59–80.
(44) Strobl, G. *The Physics of Polymers*; Springer-Verlag: Berlin, 1997..

MA702815K